https://dx.doi.org/10.4314/dujopas.v10i3b.2
ISSN (Print): 2476-8316
ISSN (Online): 2635-3490
Dutse Journal of Pure and Applied Sciences (DUJOPAS), *Vol. 10 No. 3b September 2024*

Dosimetric Response Evaluation and Structural Characterization of $(SnO)_x(TiO_2)_{1-x}$ Thin Film for Gamma Radiation Detection and Measurement

Akoso C. Christopher[1*], Umaru Ibrahim[1],Yusuf S. Dauda[1], Idris M. Mustapha[1], and Abubakar A. Mundi[1].

[1]Department of Physics,
Nasarawa State University,
Keffi
Nigeria.

Email: akosochristopher@gmail.com

Abstract

Dosimetric response evaluation as well as structural Characterization of $(SnO)_x(TiO_2)_{1-x}$ was successfully carried out using the aerosol-assisted chemical vapor deposition method. This research aimed to ascertain how X-ray radiation affected the $(SnO_2)_x(TiO_2)_{1-x}$ thin film's I-V characteristics induced current for the range (for x = 0.0, 0.3, and 0.5) in a voltage range of 0 to 8 V. The method used for developing the manufactured $(SnO_2)_x(TiO_2)_{1-x}$ thin films was aerosol assisted chemical vapour deposition. To evaluate the dosimetric response, three thin film samples with a homogeneous distribution were developed, evaluated, and analyzed. The XRD result revealed peaks that corresponded to SnO_2 and TiO_2, as well as the films' amorphous nature. With an increase in SnO_2 concentration, FESEM pictures show a reduction in crystalline size and film roughness. The thin film samples' cross-sectional FESEM image shows that the film thicknesses for TiO_2, $(SnO_2)_{0.3}(TiO_2)_{0.7}$, $(SnO_2)_{0.5}(TiO_2)_{0.5}$, and thin film are 2.33 µm, 2.73 µm, and 10.84 µm, respectively. The results of the I-V characteristics showed that electrical conductivity increased between 0 and 8 V. During irradiation with X-ray dosage (dose rate) ranging from 100 cGy (250 cGy/min) to 200 cGy (350 cGy/min) and a voltage range of 1.0 V to 8.0 V, the I-V characteristic measurements were obtained for all the thin film sensors. The current increases linearly with X-ray doses and dose rate for all thin-film sensors that are prepared for all the applied voltage. The thin films exhibit values of sensitivity (minimum detectable dose) between 7.12 x 10^{-2} and 2.74 x 10^{-3} $mA.cm^{-2}.Gy^{-1}$ (1.41 x 10^{2} - 3.65 x 10^{5} mGy). The thin film material is an essential dosimetric material because this work demonstrated that X-ray radiation could lead to changes in microstructures.

Keywords: Dosimetry, Response, Structural, Characterization, Thin Film, Gamma Radiation, Detection, Measurement.

INTRODUCTION

Generally, semiconductor radiation detectors are made of germanium or silicon (Han et al., 2022; Nie et al., 2021; Kafle et al., 2016). Large crystals are frequently used with these materials because of their superior charge transport qualities, which prevent significant carrier losses from recombination or trapping. However, one of its drawbacks is the significant thermal

Author for Correspondence

leakage current that necessitates a cryostatic environment in order to function properly. In principle, it is conceivable to detect the produced leakage current at room temperature by using other semiconductor materials with a larger band gap (>1.5 eV) that would minimize the majority of the leakage current (Doyan et al., 2021; Kamrosni et al., 2022; Liu et al., 2021). As a result, a lot of effort has been put in finding alternative semiconductor materials that at least have a high atomic number component (Doyan et al., 2021; Santos, 2022; Zerwal et al., 2021). Currently, just a few particular compound semiconductors have drawn the greatest interest as possible room-temperature radiation detectors. A bigger band gap energy and a higher probability of photoelectric absorption per unit route length (4 to 5 times higher than Ge, 100 to 200 times higher than Si) are found in thin film dosimetric material made from SnO_2 and TiO_2 individually. These properties have made the material more suitable for building a compact gamma ray detector that can operate at room temperature (Knoll, 2010).

Gamma radiation, a high-energy form of electromagnetic radiation, poses significant challenges in terms of detection and measurement due to its penetrative power and the potential for causing biological damage (Knoll, 2010). Effective gamma radiation detectors are essential in various fields, including medical imaging, nuclear power monitoring, and environmental safety (Fujishima & Honda, 1972; Faudoa-arzate et al., 2021). Traditional detection materials, while effective, often suffer from limitations such as bulkiness, high cost, and susceptibility to environmental conditions (Becker, 2014). Consequently, there is a continuous quest for new materials that offer improved sensitivity, stability, and cost-effectiveness.

SnO and TiO_2 composite thin films have drawn interest because of their special structural, electrical, and optical characteristics. Titanium dioxide is renowned for its high refractive index, chemical stability, and photocatalytic activity (Fujishima & Honda, 1972; Goto et al., 2023). On the other hand, tin oxide is valued for its electrical conductivity and transparency to visible light (Batzill & Diebold, 2005). By varying the composition of these two oxides, it is possible to tailor the properties of the thin films to meet specific requirements for gamma radiation detection (Gupta et al., 2019).

$(SnO)_x(TiO_2)_{1-x}$ thin films require structural characterisation by in-depth investigation with methods like atomic force microscopy (AFM), scanning electron microscopy (SEM), and X-ray diffraction (XRD). These methods provide insights into the crystalline structure, surface morphology, and thickness of the films, which are crucial parameters influencing their dosimetric response (Cullity & Stock, 2001; Idris et al., 2018). Additionally, understanding the interaction mechanisms between gamma photons and the thin film material is essential for optimizing their performance as radiation detectors (Aparna et al., 2022; Ali et al., 2021).

The assessment of the thin films' sensitivity, linearity, and repeatability under various gamma radiation exposure levels is known as the dosimetric response evaluation. This involves calibrating the films against known radiation sources and measuring their response using appropriate instrumentation (Sabol & Weng, 1995). Such evaluations are critical for determining the suitability of $(SnO)_x(TiO_2)_{1-x}$ thin films in practical radiation detection scenarios.

METHODOLOGY

Chemical Synthesis

Tin (II) chloride 2-hydrate ($Cl_2.Sn.2H_2O$) powder was mixed with ethanol to produce the SnO_2 precursor solution. Acetic acid is then combined with the solutions. The mixture is thereafter stirred for an hour with a magnetic stirrer until a clear solution forms.
Titanium isopropoxyde ($Ti(OC_3H7)_4$) was utilized as the TiO_2 precursor, and it was dissolved in isopropanol to create the TiO_2 precursor solution. For ten minutes at 60°C, the mixture was mixed. Following the addition of acetic acid, the new mixture was stirred for fifteen minutes. To obtain the sol-gel solution, the final mixture was agitated for two hours after the methanol was added.

The produced precursor solutions for SnO2 and TiO2 were co-doped at several mole ratios.$(SnO_2)_x(TiO_2)_{1-x}$ (x = 0, 0.3, and 0.5 wt. %) were synthesized as three distinct solutions of SnO_2-doped TiO_2 precursor solutions. In order to achieve chemical equilibrium prior to the deposition procedure, the solutions were stored at room temperature for about 24 to 48 hours.

Thin Film Deposition

The $(SnO2)_x(TiO_2)_{1-x}$ thin films were deposited by the Aerosol Assisted Chemical Vapour Deposition Method. The procedure involves producing aerosols and transferring them onto a heated soda lime glass substrate by use of compressed air acting as a carrier gas. For this research, the precursor solution was added to the dispensing tank, and a heater was used to keep the substrate temperature at 450 ^oC. The nozzle movement pattern and spray rate were set by the Repetier host software interfaced computer application.

The air flow rate, solution flow rate, and nozzle to substrate distance were all predetermined and maintained throughout the process. The spraying process was stopped once a predetermined amount of the precursor solution had been applied to the glass substrate. The substrate was removed and allowed to cool to room temperature. Using a digitally generated photo-mask, a thick layer of interdigitated graphite electrodes was formed that would serve as the electrical contacts on the prepared $(SnO_2)_x(TiO_2)_{1-x}$ thin films.

Thin Film Characterisation

The structural and phase characterizations of the deposited $(SnO_2)_x(TiO_2)_{1-x}$ thin films were performed by means of X–ray diffraction (XRD) employing Cu-K-α (λ = 1.54 Å) radiation. The divergence of the main beam was modest enough to provide the necessary resolution of low incidence glancing angle. To minimize the glass substrate contribution, XRD at grazing incidence was employed. At each step, the instrument was run in a step scan mode of 0.004, and counts were recorded for 1.91 seconds.

A scanning electron microscope (SEM) was used to study the surface morphology of the film produced with different deposition settings. Using a focused electron beam, SEM scans a surface to produce pictures. The composition and topography of the surface can be ascertained by analyzing the signals produced when the electrons in the beam make contact with the sample.

The developed materials were analyzed elementally in both bulk and thin-film form using energy dispersive X-ray (EDX) analysis. The thin film was exposed to an intense electron beam (20 KeV) during this study, which caused the specimen surface to produce distinctive X-rays. The X-ray spectrum that is released is used to ascertain the composition of every sample both

quantitatively and qualitatively, as well as to guarantee sample uniformity. Two factors led to the selection of the electron beam energy of 20 keV. The first is that the gadget can only gather a maximum of 20 keV of X-ray energy on the X-ray scale. The second rationale is to stop the film from penetrating deeply as energy levels beyond 20 keV might occur.

I-V Characteristics measurements and irradiation of the thin films

The current-voltage properties of thin-film structures exposed to varying doses of gamma-ray radiation were measured with an electrometer. For every dose of photon radiation, I-V plots were created for the samples, and the variation in the plots was computed. The mean I-V plot was taken into consideration as the typical I-V plot for each dose level. The standard I-V plots at various x-ray doses were used to obtain the current against dose graphs for each voltage applied to the coplanar structure.

The current versus dose plot, which shows the sensitivity as the change in current per unit change in photon radiation dose, was calculated for each voltage that was applied to the structure within the 0-4.8 V range. The amount of the gamma radiation dose needed to cause a change in the current of 1μA (the sensitivity of a common current dosimeter that is typically employed) in the films was computed for each applied voltage, resulting in the minimum measurable dose.

For the purpose of dosimetry, the fabricated thin films were irradiated singly to different doses of 0, 100, and 200 cGy respectively using an Electa Linear Accelerator. The irradiation area of the film was 5cm^2 and the thin film samples were mounted perpendicular to the beam. The thin films was irradiated in a sample holder with a diameter of 50 mm.

Dosimetric Fading Evaluation

To assess the functionality of the manufactured thin-film dosimeter, the tests suggested by the International Electrotechnical Commission (IEC) 1066 standard were taken into account. Following irradiation for 0, 1, 2, 15, and 30 days, the I-V characteristics were determined. The dosimeters were measured and calibrated using the radiation-irradiated dosimeter from day 0. To determine the film's stability and fading, the values that were acquired were compared.

RESULTS AND DISCUSSION

With x = 0, 0.3, and 0.5 mol%, the synthesized $(SnO_2)_x(TiO_2)_{1-x}$ thin films were prepared using an aerosol assisted chemical vapour deposition approach. In order to determine the dosimetric response, five thin film samples with a homogeneous distribution were created, characterized, and tested. The thin film samples' findings from energy dispersive X-ray spectrometry, X-ray diffraction, and field emission scanning electron microscopy were presented. The electrical properties of the films that were altered by X-ray radiation were identified and documented.

X-ray Diffraction Analysis

As a function of doping ratio (x = 0, 0.3, and 0.5 weight percent), the XRD patterns for $(SnO_2)_x(TiO_2)_{1-x}$ thin films produced by Aerosol Assisted Chemical Vapour Deposition technique were recorded. At 450˚C, the thin films were deposited on a soda lime glass substrate. The diffraction patterns are displayed in Figure 1, and all of the films have the primary characteristic peaks for TiO_2 and SnO_2 in the thin film samples in addition to the typical peaks of the substrates. The angles that (110), (101), (111), (211), and (310) correspond to are 23.96, 31.90, 39.35, 53.69, and 62.63 degrees, respectively. These are the peaks that result from pure TiO_2 thin film.

Based on the JCPDS data for TiO_2, the acquired results show good agreement with the standard results.(101), (111), (110), (202), and (121) are the peaks attributed to the TiO_2 doped SnO_2 thin film sample. These correspond to the angles 25.21, 29.71, 38.23, 48.55, and 62.87, respectively. By comparing with JCPDS data, the rutile phase structure of the peaks attributed to the SnO_2 thin film was identified. The thin film samples' XRD spectrum makes it evident that they are amorphous.

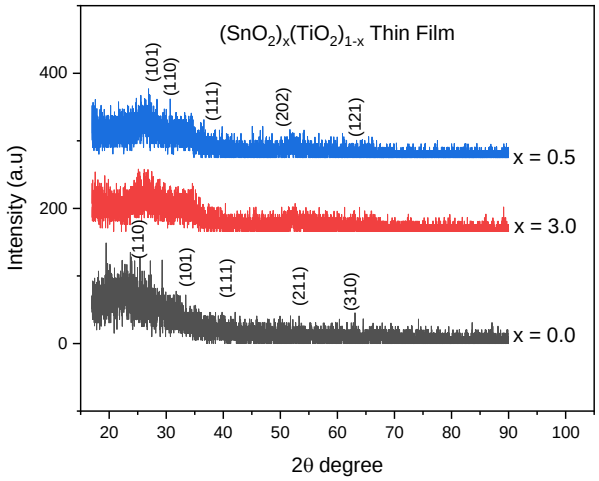

Figure 1: XRD spectra of $(SnO_2)_x(TiO_2)_{1-x}$ thin film samples.

Field Emission Scanning Electron Microscopy and Energy Dispersive X-ray Spectroscopy

As seen in Figure 2, the surface morphology of $(SnO_2)_x(TiO_2)_{1-x}$ thin films is studied using a FESEM. It is evident that pure TiO_2 thin films have a nanoscale structure, a smooth surface, and uniform crystalline grains. The film's $(SnO_2)_x(TiO_2)_{1-x}$ nanoparticles are observed to be agglomerated independently, exhibiting irregular forms and non-crystalline grains. It is discovered that when the concentration of SnO_2 rises, the grain size increases.

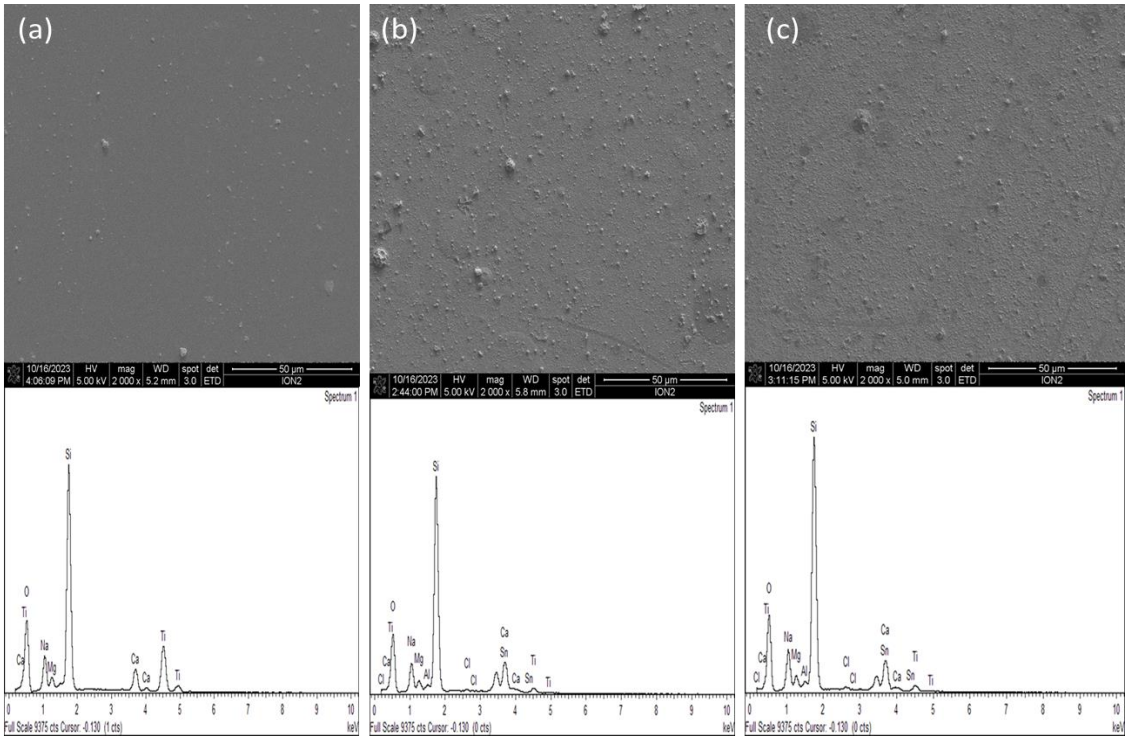

Figure 2: FESEM image with EDX spectra of $(SnO_2)_x(TiO_2)_{1-x}$ thin film sample.

It is well known that the surface morphology of the films affects their characteristics, which is crucial for uses like X-ray and gamma sensors. It is crucial to look at the surface morphology of the films since an increase in surface roughness causes the sensing characteristics of the films to rise. Figure 2 displays the EDX spectra of each of the $(SnO_2)_x(TiO_2)_{1-x}$ thin film samples together with the corresponding FESEM pictures. Following the quasi-quantitative analysis of the EDX spectrum, it was noted that the elements included in the TiO_2 thin film samples were Ti and O, whereas the elements present in the SnO_2-doped TiO_2 thin film samples were Ti, Sn, and O (Table 1).

Table 1: Elemental concentration of film, substrate and buffer layer coating elements in wt% obtained using energy dispersive X-ray spectrometry analysis.

Sample	Film element (wt%)			Substrate element (wt%)			Impurity
	Ti	Sn	O	Si	Ca	Na	Mg
TiO_2	11.56	0	46.25	29.08	4.45	6.95	1.71
$(SnO_2)_{0.3}(TiO_2)_{0.7}$	2.60	11.64	42.29	30.62	4.99	6.16	1.70
$(SnO_2)_{0.5}(TiO_2)_{0.5}$	1.66	8.37	44.34	31.48	5.20	7.14	1.81

These findings demonstrate that all of the manufactured samples had extremely low levels of magnesium contamination and high levels of purity in the produced films. Si, Ca, and Na are examples of substrate composition that are present but are not film constituents. Because the film is thin (having thicknesses of 2.33, 2.73, and 10.84 for TiO_2, $(SnO)_{0.3}(TeO_2)_{0.7}$, and $(SnO_2)_{0.5}(TiO_2)_{0.5}$ thin film samples, respectively), the electron can interact with the glass substrate, which explains why the residues of soda-lime glass substrate are relatively high in the EDX spectrum. In addition, it was noted that, in contrast to the ideal chemical stoichiometry of SnO_2 and TiO_2, the ratios of Sn/O_2 and Ti/O_2 were less than 1. These findings demonstrated that the SnO_2/TiO_2 thin film included oxygen vacancies.

I-V Characteristics Measurements

Investigations were conducted into the I-V properties of the manufactured $(SnO_2)_x(TiO_2)_{1-x}$ thin film sensors, which were found to demonstrate the variation in electrical conductivity over a range of applied voltages, 0 to 8 V. Figures 3a, 3b, and 3c illustrate the typical I-V characteristics of $(SnO_2)_x(TeO_2)_{1-x}$ thin film sensors (x = 0, 0.3, and 0.6) that were determined for the thin film sensors.

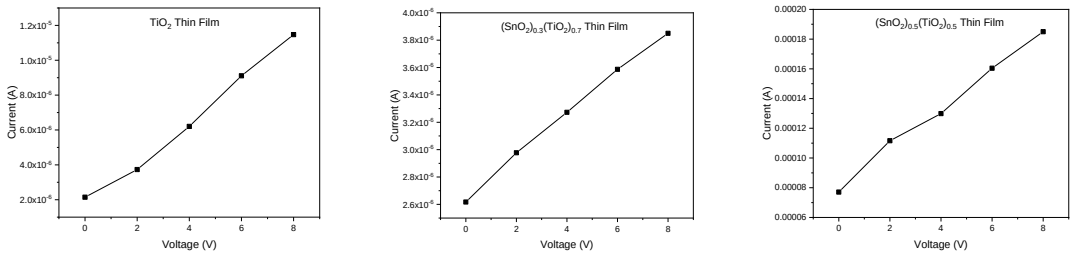

(a) TiO_2 **(b) $(SnO_2)_{0.3}(TiO_2)_{0.7}$** **(c) $(SnO_2)_{0.5}(TiO_2)_{0.5}$**

Fig. 3: I-V Characteristics measurements of thin films

It is evident from Figures 3a, 3b, and 3c that for every thin film sensor under investigation, the induced current grows linearly with an increase in applied voltage. The outcome showed how electrical conductivity changed between 0 and 8 V of applied voltage. The thin-film sensors' conductivity fell into the following order: $(SnO_2)_{0.5}(TiO_2)_{0.5} > TiO_2 > (SnO_2)_{0.3}(TiO_2)_{0.7}$.

The thin film samples' varying electrical conductivity is a good indicator of the microstructure changes brought about by the co-doping of SnO_2 and TiO_2, which in turn influences the optical, structural, and electrical characteristics of the $(SnO_2)_x(TiO_2)_{1-x}$ thin film sensor under investigation. Numerous investigations have shown that doping two or more metal oxides simultaneously can regulate the thin film sensor's semiconducting behavior (Carvalho *et al*., 2012; Rini *et al*., 2020).

X-ray Radiation Induced Changes on I-V Characteristic Measurement

In order to evaluate the dosimetric response $(SnO_2)_x(TiO_2)_{1-x}$ thin film as an X-ray and gamma sensor, the impact of X-ray radiation on the I-V characteristics was ascertained. The I-V characteristics plot at various X-ray doses for the $(SnO_2)_x(TiO_2)_{1-x}$ thin film are displayed in Figures 4(a), (b), and (c). The usual I-D curve for a $(SnO_2)_x(TiO_2)_{1-x}$ thin film sensor at various applied voltages is displayed in Figures 5a, 5b, and 5c.

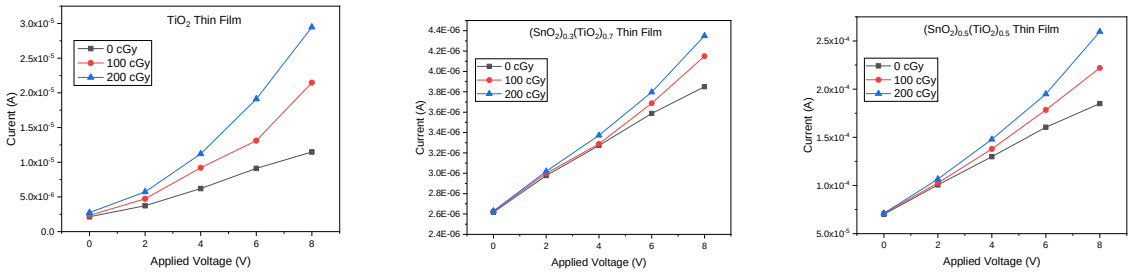

(a) TiO_2 **(b) $(SnO_2)_{0.3}(TeO_2)_{0.7}$** **(c) $(SnO_2)_{0.5}(TeO_2)_{0.5}$**

Figure 4: Typical I-V plots at different X-ray Dose for thin film sensor s

For TiO_2, $(SnO_2)_{0.3}(TiO_2)_{0.7}$, and $(SnO_2)0.5(TiO_2)_{0.5}$, respectively, the typical I-V characteristics plot determined during irradiation and at various applied voltages are shown in Figures 5 (a), (b), and (c). over every $(SnO_2)_x(TiO_2)_{1-x}$ thin film sample, the I-V characteristics measurement during irradiation was plotted over the applied voltage range of 0 - 8 V and the X-ray dosages of 0 cGy, 100 cGy, and 200 cGy. For all applied voltages in all thin film sensors, the plot indicates a linear increase in the induced current as the X-ray radiation increases.

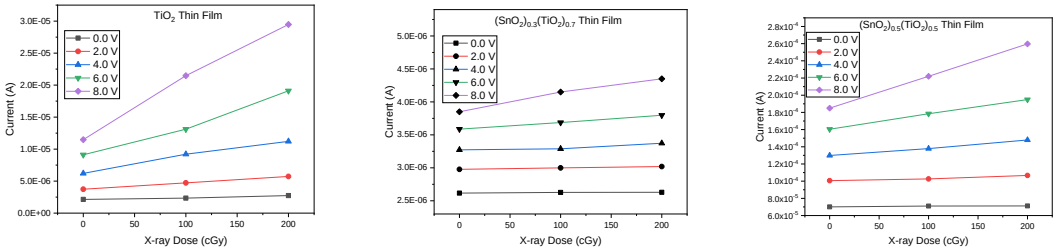

(a) TiO_2 **(b) $(SnO_2)_{0.3}(TiO_2)_{0.7}$** **(c) $(SnO_2)_{0.5}(TiO_2)_{0.5}$**

Figure 5: Typical I-D plot at different applied Voltages for thin film sensors

Table 2: Irradiation parameter and sensor dosimetric parameter of the analysed I-V characteristics results for the thin film sensor.

Sample	Irradiation Parameter			Sensor Dosimetric Parameter	
	Absorbed Dose (cGy)	Dose rate (cGy.min^{-1})	Exposure time (min)	Sensitivity (mA.cm^{-2}.Gy^{-1})	MMD (mGy)
TiO_2 Thin Film	100	250	0.40	2.34E-03	4.27E+05
	200	350	0.57	2.74E-03	3.65E+05
$(SnO_2)_{0.3}(TiO_2)_{0.7}$ Thin Film	100	250	0.40	2.63E-03	3.80E+05
	200	350	0.57	2.63E-03	3.80E+05
$(SnO_2)_{0.5}(TiO_2)_{0.5}$ Thin Film	100	250	0.40	7.11E-02	1.41E+04
	200	350	0.57	7.12E-02	1.40E+04

For TiO_2, $(SnO_2)_{0.3}(TiO_2)_{0.7}$, and $(SnO_2)_{0.5}(TiO_2)_{0.5}$, respectively, the usual current-dose (I-D) pattern at various applied voltages is displayed in Figures 5a, 5b, and 5c. The I-D plot was created for each of the $(SnO_2)_x(TiO_2)_{1-x}$ thin film samples during irradiation at X-ray dosages ranging from 0 to 200 cGy and applied voltages between 0 and 8 V. For all applied voltages in all thin film sensors, the plot indicates an increase in the induced current as the applied voltage increases.

Dosimetry Fading Evaluation

The plot of induced current against days of I-V characteristics measurements during the post-irradiation fading test of $(SnO_2)_x(TiO_2)_{1-x}$ thin films is presented in Figures 6a, 6b, and 6c. To determine the dosimetric fading of the thin film sensors, I-V characteristics measurements were performed at intervals of 0, 1, 2, 15, and 30 days following X-ray photon irradiation.

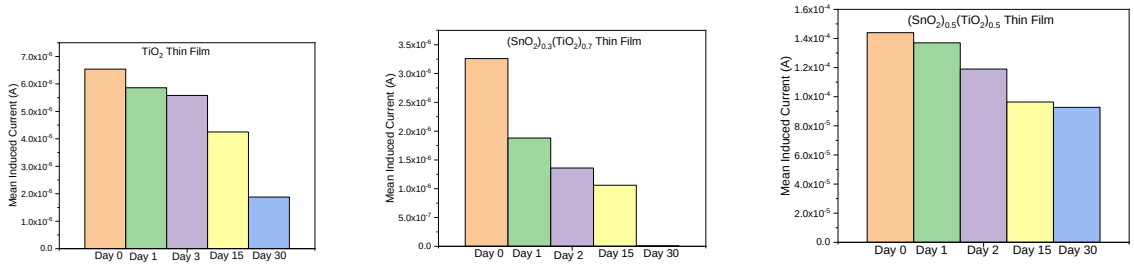

(a) TiO_2 **(b) $(SnO_2)_{0.3}(TiO_2)_{0.7}$** **(c) $(SnO_2)_{0.5}(TiO_2)_{0.5}$**

Figure 6: I-V characteristics induced current plot versus measurement days of the post-irradiation fading of thin films

The mean induced current for TiO_2 thin film on Day 0, Day 1, Day 2, Day 15, and Day 30 is displayed in Figure 6a as 6.54E-06 A, 5.86E-06 A, 5.58E-06 A, 4.25E-06 A, and 1.88E-06 A,

respectively. The assessment of I-V characteristics indicates a gradual decline over the initial three days, followed by a sharp decline after day 15. The mean induced current for the thin films of $(SnO_2)_{0.3}(TiO_2)_{0.7}$ at 3.26E-06, 1.88E-06, 1.36E-06, 1.06E-06, and BDL on Day 0, Day 1, Day 2, Day 15, and Day 30 are displayed in Figure 6b. The induced current continues after dropping off quickly.

On day 30, it was discovered that the induced current was below the detectable threshold. The mean induced current for $(SnO_2)_{0.5}(TiO_2)_{0.5}$ thin films on Day 0, Day 1, Day 2, Day 15, and Day 30 is displayed in Figure 6c as 1.44E-04, 1.37E-04, 1.19E-04, 9.64E-05, and 9.27E-05, respectively. The induced declines stabilized on days 15 and 30 after exposure, occurring gradually during the first three days. The mean induced current for $(SnO_2)_{0.7}(TiO_2)_{0.3}$ thin film is displayed in Figure 4.26 for Day 0, Day 1, Day 2, Day 15, and Day 30. The values are 0.0080238, 0.0079878, 0.0064618, 0.0062352, and 0.0062692, respectively. From day 2 to day 30, there is high stability in the induced current. For Day 0, Day 1, Day 2, Day 15, and Day 30, the mean induced current for SnO_2 thin film is 0.0133066, 0.0130886, 0.0131442, 0.0120236, and 0.0112806, respectively, as shown in Figure 6. On days 15 and 30, the induced current exhibits strong stability with minimal decline. The thin film sample fades in the following order: SnO_2 > $(SnO_2)_{0.5}(TiO_2)_{0.5}$ > TiO_2 > $(SnO_2)_{0.3}(TiO_2)_{0.7}$ at the highest order.

The findings correlate with the finding of Shamma *et al.* (2021) who investigated the potential of exploiting the properties of TiO_2 thin films as a sensing lay on MEMS–based sensors for radiation dosimetry application, the XRD result shows a change in the films from a mixture of rutile and anatase phases to an anatase phase upon irradiation.

Furthermore, the findings correlate with that of Victor (2020) who investigated the fabrication of Zn-doped SnO_2 thin films and its tuning effects by deploying the self-assembled spray pyrolysis method. The result shows a linear increase in the transient current with voltage. This study is in line with Dewi et al. (2023) who investigated the characterization of SnO/TiO_2 with the addition of polyethyene glycol via sol-gel method for self-cleaning application and obtained similar results.

The finding is also in line with Adawiyah (2017) who investigated the Structural and morphological characterization of TiO_2-SnO_2 thin film prepared by combining doctor-blade and sol-gel techniques in Indonesia, the morphological study revealed that TiO_2-SnO_2 film has more porus nature and uniform particle aggregates.

However, the finding is not in line with that of Alejandro et al. (2021) who investigated the disinfection mechanism of the photocatalytic activity of SnO_2 thin films against *Candida alicans*, the result shows a reduction of 36.5% in viable cells of albicans, also, after including SnO_2, cell viability was reduced by 60.2%. this difference could be as a result of the focus on the disinfection mechanism of the photocatalytic activities of SnO_2.

CONCLUSION

Finding out how X-ray radiation affected the I-V characteristics of the $(SnO_2)_x(TiO_2)_{1-x}$ thin film's induced current (for x = 0.0, 0.3, and 0.5) in a voltage range of 0 to 8 V was the main goal of the research work. The thin film samples that are created with the aid of a field emission scanning electron microscope and an X-ray diffractometer are smooth, homogenous, highly transparent, and possess the right electrical properties. The I-V characteristics generated current of the manufactured $(SnO_2)_x(TiO_2)_{1-x}$ thin film grows linearly with an increase in applied voltages for all thin film sensors under examination. The conductivity of the thin-film

sensors is as follows: $(SnO_2)_{0.5}(TiO_2)_{0.5}$ > TiO_2 > $(SnO_2)_{0.3}(TiO_2)_{0.7}$. The I-V characteristics measurements made during X-ray radiation exposure for each thin-film sensor under examination demonstrate that, for each applied voltage of 0–8 V, the induced current increases linearly with X-ray dose over a range of 100–200 cGy. This might be explained by changes produced to the film microstructures during the film deposition procedure on the film sample. The thin film material is a useful dosimetric material since this work shown that X-ray radiation can cause changes in microstructures. These changes are linear and relative.

REFERENCES

Adawiyah, W. R., & Pramuka, B. A. (2017). Scaling the notion of Islamic spirituality in the workplace. *Journal of Management Development, 36*(7), 877–898. https://doi.org/10.1108/JMD-11-2014-0153

Alejandro, A., Oscar, H. F., Lyda Z. R., & Peter, F. R. (2021). Photocatalytic Activity and Antibacterial Behavior of Fe3+-Doped TiO2/SnO2 Nanoparticles. *Energy Research Journal, 1*(2), 120-125.

Ali, G. A., Emam-Ismail, M., El-Hagary, M., Shaaban, E. R., Moustafa, S. H., Amer, M. I., & Shaban, H. (2021). Optical and microstructural characterization of nanocrystalline Cu doped ZnO diluted magnetic semiconductor thin film for optoelectronic applications. *Journal of Optical Materials, 119*(June), 111312. https://doi.org/10.1016/j.optmat.2021.111312

Aparna, C., Shetty, P. K., & Mahesha, M. G. (2022). Structural optimization of indium oxide thin film for gamma dosimetry applications. *Journal of Materials Science in Semiconductor Processing, 150*, 106931.

Batzill, M., & Diebold, U. (2005). The surface and materials science of tin oxide. *Progress in Surface Science, 79*(2-4), 47-154. https://doi.org/10.1016/j.progsurf.2005.09.002

Becker, K. (2014). *Radiation detectors: Physical principles and applications*. Oxford University Press.

Carvalho, D. H. Q., Schiavon, M. A., Raposo, M. T., Paiva, R. De, Alves, J. L. A., Paniago, R. M., Speziali, N. L., Ferlauto, A. S., & Ardisson, J. D. (2012). Synthesis and characterization of SnO2 thin films prepared by dip-coating method. *Journal of Physics Procedia, 28*(1), 22–27. https://doi.org/10.1016/j.phpro.2012.03.664

Cullity, B. D., & Stock, S. R. (2001). *Elements of X-ray diffraction* (3rd ed.). Prentice Hall.

Dewi, Y. S., Arifin, H., Pradipta, R. O., Qona'ah, A., Rosita, R., Giatin, C. N., & Gauda A. D. K. (2023). Efficacy of Intermittent and Continuous Subglottic Secretion Drainage in Preventing the Risk of Ventilator-Associated Pneumonia: A Meta-Analysis of Randomized Control Trials. *Medicina, 59*(11), 283.

Doyan, A., Alam, K., Muliyadi, L., Ali, F., & Awang, M. M. (2021). Synthesis and Characterization of SnO2 Thin Film Semiconductor for Electronic Device Applications. *Jurnal Penelitian Pendidikan IPA, 7*(1), 2017–2021. https://doi.org/10.29303/jppipa.v7iSpecialIssue.1270

Faudoa-arzate, A., Camarillo-cisneros, J., Castillo-gonzález, A. R., Favila-pérez, M. A., Sáenz-hernández, R. J., Realyvazquez-guevara, P. R., & Arzate-quintana, C. (2021). Disinfection mechanism of the photocatalytic activity of SnO2 thin films against Candida albicans, proposed from experimental and simulated perspectives. *Canadian Journal of Microbiology, 676*(June), 667–676.

Fujishima, A., & Honda, K. (1972). Electrochemical photolysis of water at a semiconductor electrode. *Nature, 238*(5358), 37-38. https://doi.org/10.1038/238037a0

Goto, S., Hayashi, H., Yamaguchi, H., Sekiguchi, H., & Akino, R. (2023). Signal-stabilized Al2O3 : C-OSL dosimeter "checking chip" for correcting OSL reader sensitivity variation. *160(May 2022)*, 5–11.

Gupta, R., Chauhan, R. P., & Kumar, R. (2019). Influence of gamma radiation on the optical, morphological, structural and electrical properties of electrodeposited lead selenide nanowires. *Journal of Optical Materials, November*, 109538. https://doi.org/10.1016/j.optmat.2019.109538

Han, B., Park, M., Kim, K., & Lee, Y. (2022). Characterization of Flexible Amorphous Silicon Thin-Film Transistor-Based Detectors with Positive-Intrinsic-Negative Diode in Radiography.

Idris, M. M., Olarinoye, I. O., Kolo, M. T., & Ibrahim, S. O. (2022). Transparent Conducting Oxides Thin Film Dosimetry: Present and the Future. *Journal of Radiation and Nuclear Applications, 7*(1), 49–58.

Kafle, B. P., Pokhrel, B. R., & Lamichhane, P. (2016). Thickness Dependence of Optical and Electrical Properties of Zinc Oxide Thin Films. *SOJ Materials Science and Engineering, 4*(1), 117–120. http://dx.doi.org/10.15226/sojmse.2016.00119

Kamrosni, A. R., Suryani, C. H. D., Azliza, A., Mustafa, A. B. A. M., Anuar, M. S. M. A., Norsuria, M., Chobpattana, V., Kaczmarek, L., Jeż, B., & Nabiałek, M. (2022). Microstructural Studies of Ag/TiO2 Thin Film; Effect of Annealing Temperature. *J. Arch. Metall. Mater., 67*(1), 241–245.

Knoll, G. F. (2010). *Radiation detection and measurement* (4th ed.). John Wiley & Sons.

Liu, Y., Song, Z., Hu, M., Chen, J., Yuan, S., & Xu, L. (2021). Self-powered adjustable UV and NIR photodetectors based on one-step synthesized TeO2 doped ZnO composite nanorods/Si heterojunction. *Sensors and Actuators, A: Physical, 331*, 113009. https://doi.org/10.1016/j.sna.2021.113009

Nie, Y., Xie, Y., Zheng, Y., Luo, Y., Zhang, J., Yi, Z., Zheng, F., Liu, L., Chen, X., Cai, P., & Wu, P. (2021). Preparation of ZnO/Bi2O3 composites as heterogeneous thin film materials with high photoelectric performance on FTO base. *Journal of Coatings, 11*(9). https://doi.org/10.3390/coatings11091140

Rini, A. S., Deraf, M. P., & Hamzah, Y. (2020). Optical, structural and morphological studies of TiO2 thin film synthesized by liquid phase deposition method. *AIP Conference Proceedings, 080015*(May).

Santos, L. A. P. (2022). An Overview on Bipolar Junction Transistor as a Sensor for X-ray Beams Used in Medical Diagnosis. *Sensors, 22*, 1–28.

Sabol, J. M., & Weng, P. S. (1995). *Introduction to radiation protection dosimetry*. World Scientific.

Shamma, K., Aldwayyan, A., Albrithen, H., & Alodhayb. (2021). Exploiting the properties of TiO2 thin films as a sensing layer on (MEMS)-based sensors for radiation dosimetry applications. *AIP Advances, 025209*(February), 1–9. https://doi.org/10.1063/5.0032353

Victoria, D. C. B. (2020). Fabrication of ZN Doped SnO2 Thin Films and its Tuning Effects. *International Journal of Advanced Research in Engineering and Technology, 11*(11), 1490–1498.

Zerwal, A. P., Khadayate, R. S., Malpure, N. N., Kasar, C. K., & Marathe, D. M. (2021). TiO2 Thin Films: A Review. *International Journal of Innovative Research in Technology, 8*(7), 563–569.